CORA Cork Open Research Archive
Cartlann Taighde Oscailte Chorcaí

Title	Ultra-high negative infrared photoconductance in highly As-doped germanium nanowires induced by hot electron trapping
Authors	John, John Wellington;Dhyani, Veerendra;Georgiev, Yordan M.;Gangnaik, Anushka S.;Biswas, Subhajit;Holmes, Justin D.;Das, Amit K.;Ray, Samit K.;Das, Samaresh
Publication date	2020-06-30
Original Citation	John, J. W., Dhyani, V., Georgiev, Y. M., Gangnaik, A. S., Biswas, S., Holmes, J. D., Das, A. K., Ray, S. K. and Das, S. (2020) 'Ultrahigh Negative Infrared Photoconductance in Highly As-Doped Germanium Nanowires Induced by Hot Electron Trapping', ACS Applied Electronic Materials, 2(7), pp. 1934-1942. doi: 10.1021/acsaelm.0c00245
Type of publication	Article (peer-reviewed)
Link to publisher's version	https://pubs.acs.org/doi/full/10.1021/acsaelm.0c00245 - 10.1021/acsaelm.0c00245
Rights	© 2020 American Chemical Society. This document is the Accepted Manuscript version of a Published Work that appeared in final form in ACS Applied Electronic Materials, copyright © American Chemical Society after peer review and technical editing by the publisher. To access the final edited and published work see https://pubs.acs.org/doi/full/10.1021/acsaelm.0c00245
Download date	2024-04-26 23:09:06
Item downloaded from	https://hdl.handle.net/10468/10476

UCC
University College Cork, Ireland
Coláiste na hOllscoile Corcaigh

Ultra-High Negative Infrared Photoconductance in Highly As-doped Germanium Nanowires Induced by Hot Electron Trapping

John Wellington John[ɔ], Veerendra Dhyani[ɔ], Yordan M. Georgiev [#, ¥,£] , Anushka S. Gangnaik[#], Subhajit Biswas[#], Justin D. Holmes [#], Amit K. Das[$], Samit K. Ray[€], Samaresh Das[ɔ*]

[ɔ]*Centre for Applied Research in Electronics, Indian Institute of Technology Delhi, New Delhi 110016, India*

[#] *School of Chemistry and AMBER Centre, University College Cork, Cork, T12 YN60, Ireland.*

[¥]*Institute of Ion Beam Physics and Material Research, Helmholtz-Zentrum Dresden-Rossendorf, Bautzner Landstraße, 400, 01328, Dresden, Germany*

[£]*Institute of Electronics at Bulgarian Academy of Sciences, 72, Tsarigradsko Chausse Blvd., 1784 Sofia, Bulgaria*

[$]*Laser Material Processing Division, Raja Ramanna Centre for Advanced Technology, Indore 452 013, India*

[€]*S.N Bose National Centre for Basic Sciences, Salt Lake City, Kolkata – 700106, India*

ABSTRACT: Here we report the observation of negative photoconductance (NPC) effect in highly arsenic doped germanium nanowires (Ge NWs) for the infrared light. NPC was studied by light assisted Kelvin probe force microscopy (KPFM), which shows the depletion of carriers in n-Ge NW in presence of infrared light. The trapping of photo-carriers leads to high recombination of carriers in presence of light, which is dominant in the n-type devices. Furthermore, carrier trapping model was used to investigate the trapping and detrapping phenomena and it was observed that the NPC in n-Ge occurred due to the fast trapping of mobile charge carriers by interfacial states. The performance of n-type devices was compared with p-type NW detectors, which shows the conventional positive photoconductive behavior with high gain of 10^4. The observed results can be used to study the application of Ge NWs for various optoelectronic applications involving light tunable memory device applications.

KEYWORDS: *Negative Photoconductivity, Infrared detection, hot electron trapping, Germanium Nanowire, Diameter-dependent photoconductance*

INTRODUCTION

Numerous studies utilized positive photoconductance (PPC) in bulk semiconductor materials[1, 2], thin films[3, 4], quantum dots[5, 6] and nanowires[7, 8] for a range of photovoltaic and optoelectronic device applications. However, negative photoconductivity (NPC), an unconventional photo-excitation phenomenon in which the photocurrent is lower than the dark current, has recently been observed in different semiconductors, attributed to trapped charges and surface effects. NPC has been found in large band-gap materials like AlN[9], p-ZnSe[10], GaO_3[11], and is described by the phenomenon of sub-bandgap excitation. In these materials, NPC occurs due to the abduction of free electrons as a result of photoexcitation by trap states, both extrinsic and intrinsic, in the middle of their bandgap. The presence of interfacial charges in nanoparticles of metals can also lead to the NPC effect[12].

Recently, negative photoconductance in narrow bandgap InAs nanowires was observed due to the depletion of conduction channels by light assisted hot electron trapping[13]. A similar NPC behavior has also been reported in a highly doped silicon nanowire FET under illumination of visible light[14]. In both of these cases, NPC occurred due to interfacial states and hot electron trapping by dopant ions. The competitive electron transient between trapping in interfacial states and fast recombination of electrons has been shown to depend on the doping concentration[13, 14].

Germanium, particularly in nanostructure form, has been studied extensively for photodetection applications due to its high electron and hole mobilities[15, 16]. As silicon cannot be used for C band optical communication for infrared range and III-V materials integrated in Si is costly and complicated, germanium on insulator can replace these in field of communication[17]. Single germanium nanowire photodetectors have always shown excellent responsivity (10^7) and high internal gain (~10^3) in the infrared range[18, 19]. Diameter dependent photoconductive gain is also studied to imply its application in nano-optoelectronics[20]. Using nanostructures for photodetection provides many added advantages like surface effect, which arises from their large surface-to-volume ratio and plays an important role in dominating the electrical characteristics. The free electrons released due to photon-assisted excitation are strongly affected by carrier trapping and/or scattering at the surface localized energy states compared to bulk energy states[16,21,22]. In some cases, in highly doped areas, these are responsible for delays in photocarrier recombination by hole trapping at surface states which leads to an enhancement in photoconductive gain and an increase in lifetime[7]. The first reported work on NPC in germanium

bulk material attributed this phenomenon to the capturing of majority carriers from photothermal excitation by shallow levels[23]. This happens when the contact distance between the two electrodes is larger than the traveling distance of majority carriers before being captured. To the best of our knowledge, the NPC phenomenon in highly doped n-type NWs in the infrared region is not reported yet.

Here, we present a detailed study of diameter dependent negative photoresponse of n-type germanium nanowire devices along with the photoconductive behavior of p-type nanowire in the infrared range up to 1550 nm of light illumination The familiar case of PPC occurs due to the free electrons escaping the valance band when the energy of the incident light is greater than the bandgap of the material. Whereas, NPC develops because of the hot electrons being trapped at the interfacial states by the dopant ions and also the surface traps states present in the conduction band. The KPFM analysis was done to measure the surface potential in the NWs and the reverse phenomena was observed indicating the negative photoconductance. This phenomenon is generally expected in high doped n-type semiconductors where under illumination, the majority carriers (electrons) are trapped by the surface states and donor states. The larger detrapping time of electrons than the trapping time accelerates the recombination process of photo-carriers and thus reduces the conductivity of the NWs.

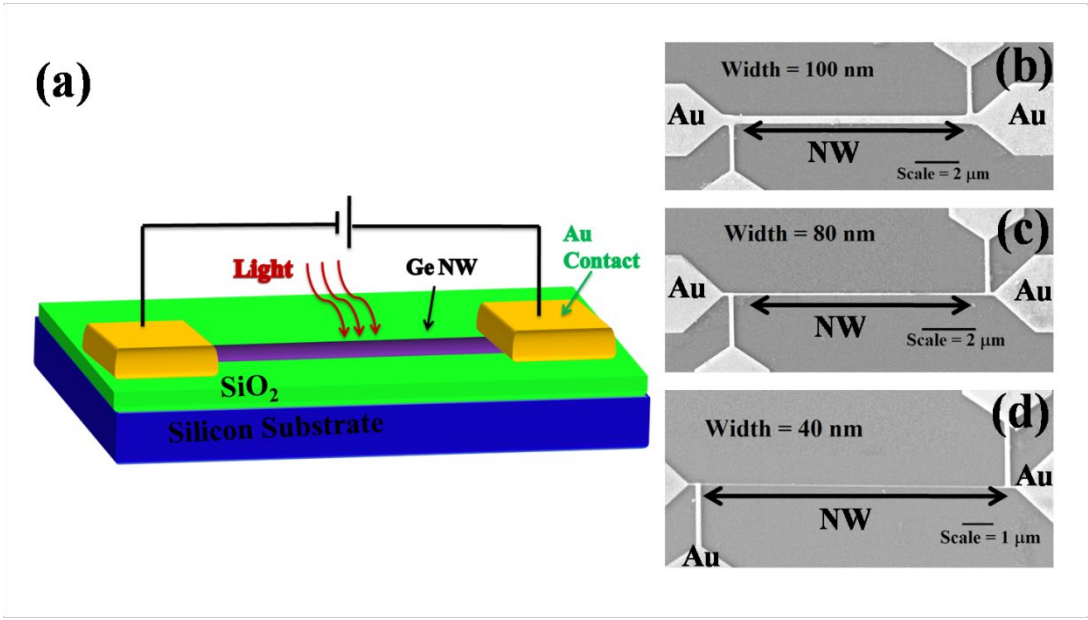

Fig. 1. Fabricated Ge NW MSM photodetector. **a** Schematic view and **b-c** SEM image of nanowires of width (**b**) 100 nm, (**c**) 80 nm, and (**d**) 40 nm.

DEVICE FABRICATION AND ELECTRICAL CHARACTERIZATION

P-type and n-type NWs were fabricated from Ge on insulator (GeOI) wafers with top Ge thickness of 50 nm through top-down approach. The wafers were cleaned by deionized water containing 0.5% of HF. A fine oxide layer formed by dipping in a solution of H_2O_2 and deionized water. Later, this oxide is removed by diluted HF dip. Boron and Arsenic doping were done with Ion Implantation technique. NWs were patterned using Electron Beam Lithography and unexposed resist were removed using developer solution. The substrates were cleaned again to remove any residues. Anisotropic etching was done for 30 seconds in Reactive Ion Etching with SF_6 and oxygen gas with a 10:1 ratio in 40 W rf power. Width of the p-type nanowire was 100 nm and the length was 10 μm and the width of the n-type nanowires was varied to 100 nm, 80 nm and 40 nm keeping the length constant at 10 μm. The substrate was again cleaned and was patterned for defining contact electrodes through optical lithography. The contacts were made by depositing Cr/Au (90 nm thick) by RF sputtering and then patterned by liftoff to for a Metal-Semiconductor-Metal (MSM) device. Keithley semiconductor parameter analyzer (SCS4200) was used to perform electrical characterization and a Thorlab's fiber-coupled multi-channel light source (MCLS1**)** was used as light source. For wavelength-dependent measurements, Thorlab's Fiber-Coupled Light Source (SLS201) was used**.** The light used for the entire measurements was having a spot size of 3 mm diameter. The schematic representation and SEM image of the devices are shown in Fig. 1.

The current-voltage characteristics of n-type Ge NWs of different diameters and p-type Ge NW device with a diameter of 100 nm are shown in Fig. 2. Under the exposure of 1550 nm light with different optical powers, highly doped n-type Ge-NW devices displayed a negative photoresponse. Here, decreasing the diameter of the nanowire resulted in a decrease in the dark current and an increase in negative photoresponse. Maximum negative photoresponse was observed in the Ge NW with a diameter of 40 nm. The photoresponse is inversely proportional to NW diameter due to the larger number of surface states with respect to the total nanowire volume with decreasing diameter. The obtained trend in diameter dependent negative response for n-type Ge NW agrees with the positive response of the Ge NW photodetectors shown in earlier works[20, 24]. Fig. 2 (d) shows the response of a p-type NW. In comparison with the n-type NWs, p-type Ge-NW showed a positive photoresponse for the same wavelength and optical power.

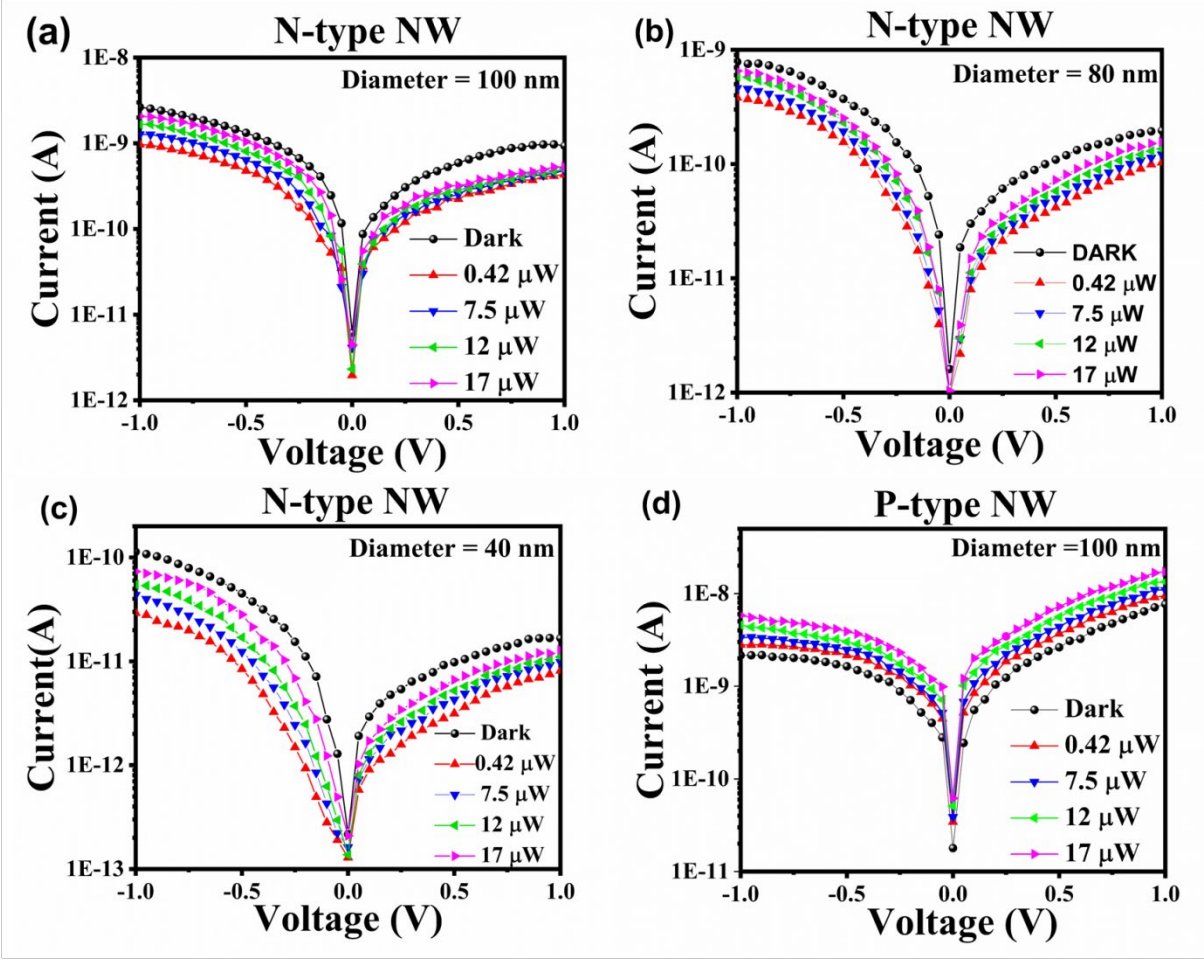

Fig. 2. I-V characteristics of n-type Ge nanowires showing the decrease in photocurrent with increasing power for varying diameter **a** 100 nm, **b** 80 nm, **c** 40 nm and **d** p-type Ge nanowire with a diameter 100 nm in dark and under illumination showing an increase in photocurrent with increasing optical power for the light of wavelength 1550 nm.

Interestingly for the n-type NWs, as the intensity of the illuminated light is increased, the negative change in photocurrent decreases, whereas for p-type NW, the photocurrent increases with intensity of light. In the case of n-type NWs, the free electrons released as a result of photon excitation, are trapped by the defect states in the conduction band, which reduces the total conductivity of the device. The electrons after getting trapped give rise to a photocurrent which is further lower than the dark current. As the incident light intensity is increased, the effect of trapping is decreased and the negative photocurrent change is reduced due to the increase in amount of free electrons. In contrast to the n-type Ge NWs, the p-type NWs show the "traditional" positive photoconductive effect. The photo-excited free majority carriers in the

device lead to an increase in photocurrent. Here, the holes are the majority carriers and cannot be trapped by trap states which results in a positive response compared to n-type NWs. The photocurrent increases upon increasing the intensity of the incident light at a wavelength of 1550 nm, since more charge carriers are released at higher light intensities.

The relative change in current as a function of different light intensity at the same wavelength (1550 nm) is shown in Fig. 3 for n-type NWs and p-type NW. The relative change in current[14] for a NW is given by the equation (1),

$$\Delta I(\%) = \frac{(I_{light} - I_{dark})}{I_{dark}} \text{ x } 100 \qquad (1)$$

The negative photoconductive effect gradually increases with increase in intensity of the incident light. After a certain intensity of 0.4 μW/cm^2, due to increased number of free electrons, the change in photocurrent is reduced significantly. Three sets of devices for each nanowire dimension was fabricated which replicated the results with an error of ± 3%. The change in NW width also gives the same trend in photocurrent change. For current measured at different intensities of light, the photocurrent was always below the dark current value, which suggests that the number of trap states was high. The negative change was higher for nanowires with diameters around 40 nm, compared to those with diameters of 80 and 100 nm. For p-type nanowires the photocurrent increases with the light intensity and start to saturate for larger light intensity (above 70 μW/cm^2) as shown in Fig. 3 (b).

Huge change in photocurrent for small change in intensity of light can be helpful in designing non-volatile memory devices which requires low power consumption[13, 25]. When illuminated, the device induces a negative photoconductivity and when the light is turned OFF, the initial current level (dark current) is achieved very slowly due to high detrapping current. This gives a high conductance ratio of high resistive state and low resistive state in a memory device. As the Ge NW can operate in near infrared range, it can be used in communication devices for the wavelength range of 800 nm to 1550 nm.

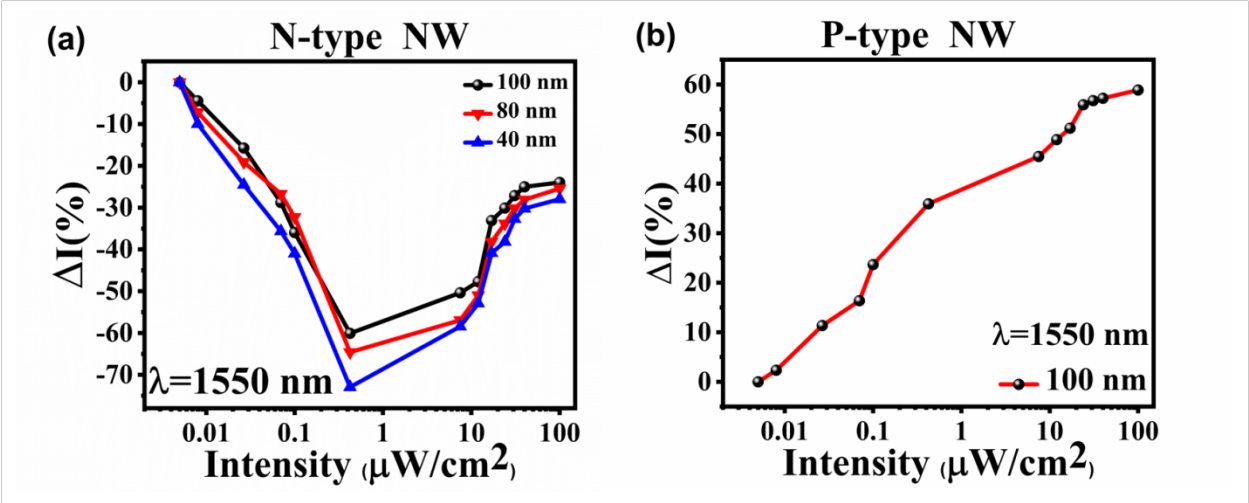

Fig. 3. Relative change in photocurrent as a function of light intensity. **a** n-type NWs showing increase in NPC with increasing intensity till 0.4 μW/cm^2 and the gradual decrease thereafter, and **b** p-type nanowires showing increase in photocurrent with increase in intensity of light.

DISCUSSION

KPFM analysis. Inorder to understand the mechanism of light-induced hot electrons trapping in the n-type NWs, the surface potential was measured using Kelvin probe force microscopy (KPFM) in dark and light illumination. Atomic force microscopy (AFM) setup of SCM-PIT from Bruker, Inc., USA, was used for KPFM measurements. Pt-Ir coated cantilever was used as the AFM tip. In KPFM mode, the normal microscopic lights were turned OFF to measure the contact potential difference (CPD) of the NWs in dark conditions. For illumination, infrared light was provided externally through an optical fiber which incident with a spot size of diameter 5 mm in the substrate. The scan area was fixed to 2 μm in the surface of the NW. KPFM mode in an AFM setup was used for the characterization, which measures the difference of potential between the tip and the sample. Any physical or chemical changes reflect as a change in the surface potential. The light was provided through an optical fiber externally to the measurement setup. Fig. 4 shows the topology and surface potential of the n-type and p-type nanowires. Fig. 4 (a) and (b) show the AFM topography in dark and light conditions for n-type NW, where (e) shows the variation in surface potential of the same. Fig. 4 (c) and (d) represents p-type NW in dark and light and its surface potential variation is given by (f). For any semiconductor, light illumination will cause photo-generated electrons/holes to accumulate at the surface depending upon the

nature of doping[26, 27]. This accumulation of electrons/holes enlarges the CPD for n-type and reduces the CPD for p-type when the work function of the tip is higher than that of the sample. In our case, the measured CPD decreases with the illumination of light for n-type NWs, which is contradictory to conventional PPC behavior [26, 27] due to depletion of charge carriers. From Fig. 4 (e), we can see that the maximum CPD value for the dark condition is around 13 mV in the NW while the light is lowered to -3 mV. For p-type NW the average CPD values are 18 mV and -4 mV for dark and light conditions respectively which are shown in Fig. 4 (f). There is a very small difference between CPD observed at the centre and edges of the NW (1-3 meV), which may be due to measurement error in KPFM, as when the KPFM probe will scan the edges it may have some measurement offset which is different at centre due to height change.

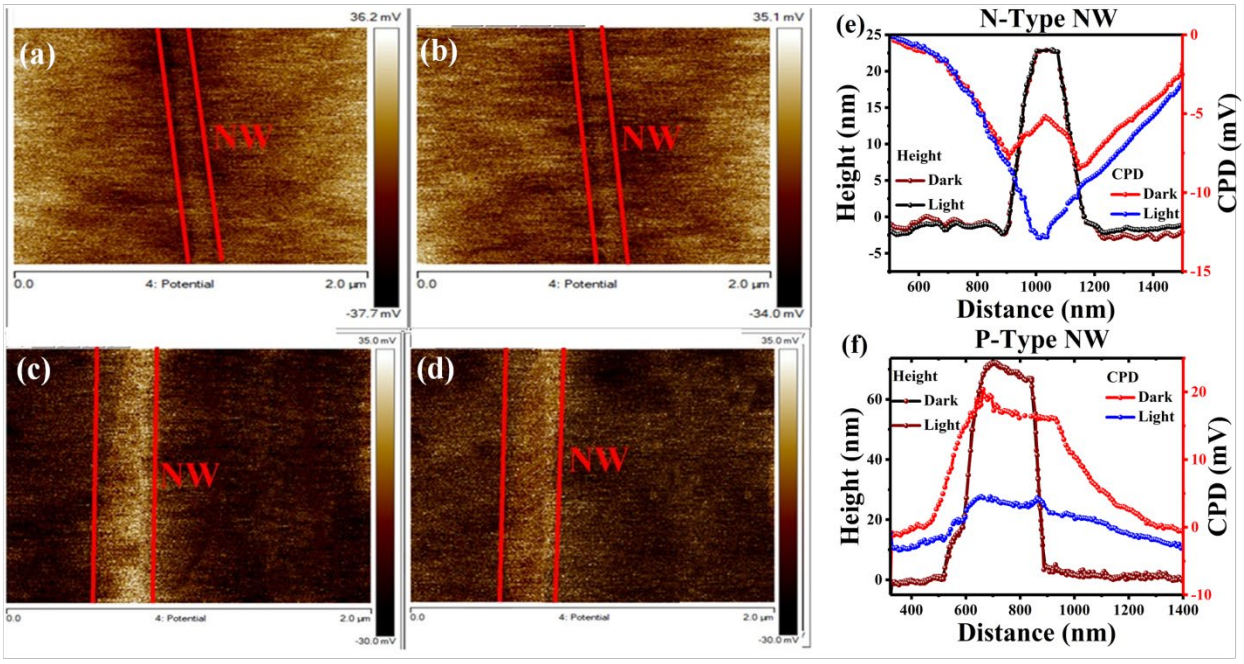

Fig. 4. KPFM analysis. Topology of n-type Ge NW in **a** dark, and **b** light conditions and p-type NW in **c** dark, and **d** light conditions. CPD for dark and light conditions. **e** n-type Ge NW and **f** p-type Ge NW.

Hot electrons are the one with kinetic energy and are generated when high energy of light is illuminated in the NW. The mean free path for the doping concentration of 10^{19} cm^{-3} with a mobility[28] of 20 cm^2/V s is ~ 106 nm. This mean free path is higher than the nanowire width and height. Therefore we can say that even for the low energy photons the mean free path is comparable to nanowire size. It is possible that, for the photons of energy 0.8 eV, electrons can

reach out to the surface states and get trapped, which can give rise to NPC. When infrared light is illuminated, the photogenerated holes will trap the electrons, decreasing the number of free electrons in the NW and increasing the work function difference. Thus, CPD is being lowered compared to that of dark condition. Whenever there is a voltage applied to the tip of the cantilever, there will be a CPD equal to $(\Phi_{tip} - \Phi_{sample})/e$ where ϕ defines the work function and e, the elementary charge. The lowering of the CPD indicates the decrease in electrons in the sample. A deep look into the band diagram shown in Fig. 5 will further help us to understand the phenomenon of the NPC and PPC from the theory of KPFM. Fig. 5 (a) shows the band diagram of a highly doped n-type Ge nanowire. As the germanium doping is very high (1 x 10^{19} cm^{-3}), it act as a degenerated semiconductor and the Fermi level energy (E_F) is above the conduction band (E_c) for n-type due to excess of electrons and below the valance band (E_v) for the p-type NW due to excess of holes. The work function difference between the sample (Φ_n) and the tip of the cantilever (Φ_{tip}) is given by $\Phi_{tip} - \Phi_n$. When the sample is illuminated, free electrons are generated and are trapped by the surface traps and thus the total number of electrons decreases. This forces the Fermi level of the sample below the conduction band energy ($\Phi`_n$) (Fig. 5 (b)). Reduction in CPD ($\Phi_{tip} - \Phi`_n$) from the light-induced KPFM analysis is justified by the above fact. In case of p^{++} Ge NW, the Fermi level is below the valence band and represented by Φ_p (Fig. 5 (c)). With the illumination of light, the free electrons are released and thus the number of holes will also increase, which changes Fermi level work function to $\Phi`_p$. Usually, the hot electrons generated are responsible for the electron trapping rather than the hot holes[29]. Therefore in p-type NW, the electrons are not confined in trap states. This induces a reduction in $\Phi_p$ which in turn reduces the CPD level ($\Phi_{tip} - \Phi`_p$), which is reflected by Fig. 5 (d) in the band diagram and Fig. 4 (f) in the KPFM analysis.

This can be further explained by the Fermi level energy and the non-equilibrium electron density relationship given by the equation (2)[26]

$$n = N_c \exp\left[-(E_c - E_F^{`})/k_B T \right] \quad (2)$$

and the quasi-Fermi level of n-type can be expressed as

$$E_F^{`} = E_c + k_B T \left(\ln n - \ln N_c\right) \quad (3)$$

where, N_C is the conduction band density of states, E_c the bottom of the conduction band, and k_B the Boltzmann constant. The upward and downward shift of the Fermi level from the equilibrium

contributes to the Quasi Fermi Level resulting in the CPD change. In contradiction to the ideal n-type NW materials, the device is showing a shift in the downward direction, which is responsible for the lowering of CPD.

The negative photoconductivity can be further explained on the basis of trapping of photogenerated electrons in the trap states[13, 14]. The hot electron density responsible for the trap states can be given by the following relations of carrier trapping model[13]:

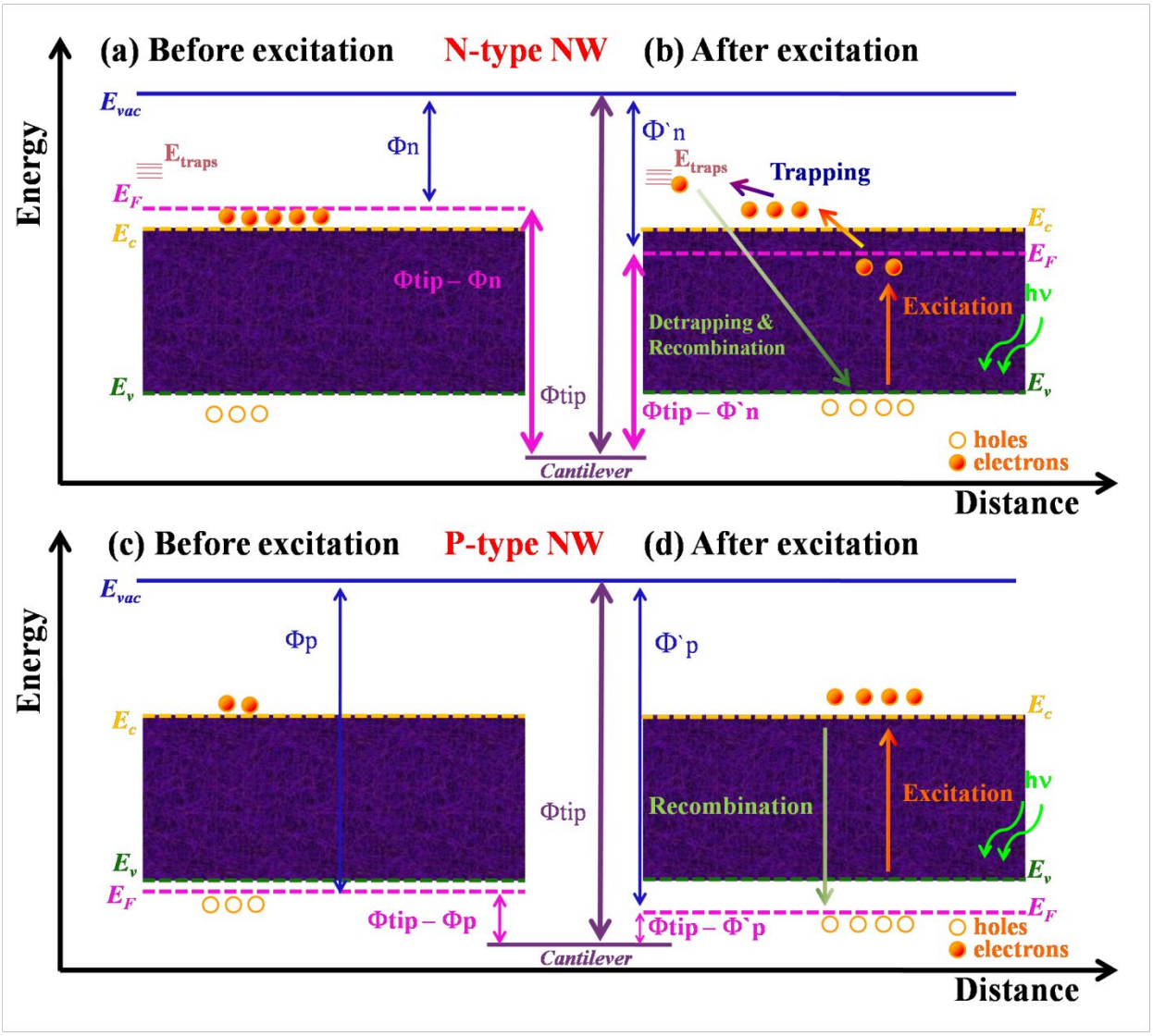

Fig. 5. Band diagram of Ge NW. For n-type NWs under **a** dark condition, **b** light illumination and for p-type NWs under **c** dark condition, **d** light illumination.

$$\frac{dn_{hot}}{dt} = G - \frac{n_{hot}}{\tau_{th}} - \frac{n_{hot}}{\tau_{trp}}\left(1 - \frac{n_{trp}}{N_{trp}}\right) \quad (4)$$

$$\frac{\mathrm{d}n_{\mathrm{trp}}}{\mathrm{d}t} = \frac{n_{\mathrm{hot}}}{\tau_{\mathrm{trp}}}\left(1 - \frac{n_{\mathrm{trp}}}{N_{\mathrm{trp}}}\right) - \frac{n_{\mathrm{trp}}}{\tau_{\mathrm{dtrp}}} \tag{5}$$

$$\frac{\mathrm{d}\Delta n}{\mathrm{d}t} = \frac{n_{\mathrm{hot}}}{\tau_{\mathrm{th}}} - \frac{\Delta p}{\tau_{\mathrm{r}}} + \frac{n_{\mathrm{trp}}}{\tau_{\mathrm{dtrp}}} \tag{6}$$

$$\frac{\mathrm{d}p_{\mathrm{hot}}}{\mathrm{d}t} = G - \frac{p_{\mathrm{hot}}}{\tau_{\mathrm{th}}} \tag{7}$$

$$\frac{\mathrm{d}\Delta p}{\mathrm{d}t} = \frac{p_{\mathrm{hot}}}{\tau_{\mathrm{th}}} - \frac{\Delta p}{\tau_{\mathrm{r}}} \tag{8}$$

Where n_{hot}, p_{hot}, n_{trp}, N_{trp}, Δn, Δp are the densities of hot electrons, hot holes, trapped electrons, trap states, excess electrons and excess holes respectively. τ_{th}, τ_{r}, τ_{trp}, τ_{dtrp} are respectively the carrier thermalization time, recombination time, trapping and de-trapping time. G is the photogeneration rate per unit volume. In low-intensity photoexcitation, the number of trapped electrons will be much lower as compared to the trap states i.e. $n_{\mathrm{trp}}/N_{\mathrm{trp}} << 1$. With this assumption, the above set of differential equations can be solved analytically to obtain the temporal dependence of various carrier densities. For the photocurrent recovery process after switching off the illumination at t = 0, we obtain,

$$n_{\mathrm{hot}}(t) = \frac{G\tau_{\mathrm{th}}\tau_{\mathrm{trp}}}{\tau_{\mathrm{th}} + \tau_{\mathrm{trp}}} \exp(-[1/\tau_{\mathrm{th}} + 1/\tau_{\mathrm{trp}}]t) \tag{9}$$

$$n_{\mathrm{trp}}(t) = \frac{G\tau_{\mathrm{dtrp}}\tau_{\mathrm{th}}}{(\tau_{\mathrm{th}} + \tau_{\mathrm{trp}})} \exp\left(-\frac{t}{\tau_{\mathrm{dtrp}}}\right) + \frac{G\tau_{\mathrm{th}}}{(\tau_{\mathrm{th}} + \tau_{\mathrm{trp}})} \frac{1}{\left(1/\tau_{\mathrm{dtrp}} - 1/\tau_{\mathrm{th}} - 1/\tau_{\mathrm{trp}}\right)} \left[\exp(-[1/\tau_{\mathrm{th}} + 1/\tau_{\mathrm{trp}}]t) - \exp(-t/\tau_{\mathrm{dtrp}})\right]$$

$$p_{\mathrm{hot}} = G\tau_{\mathrm{th}} \exp(-t/\tau_{\mathrm{th}}) \tag{10}$$

$$\Delta p = G\tau_{\mathrm{r}}\left[\frac{\tau_{\mathrm{r}}}{\tau_{\mathrm{r}} - \tau_{\mathrm{th}}} \exp(-t/\tau_{\mathrm{r}}) - \frac{\tau_{\mathrm{th}}}{\tau_{\mathrm{r}} - \tau_{\mathrm{th}}} \exp(-t/\tau_{\mathrm{th}})\right] \tag{11}$$

$$\Delta n = \Delta p + p_{\text{hot}} - n_{\text{hot}} - n_{\text{trp}} \tag{12}$$

Assuming electron mobility (μ_n) to be much higher than hole mobility, the change in conductivity at time t is,

$$\Delta\sigma(t) = (\Delta n + n_{\text{hot}})e\mu_n \tag{13}$$

The change in current is proportional to the change in conductivity. Hence, we can write

$$\frac{\Delta I(t)}{\Delta I(0)} = \frac{\Delta\sigma(t)}{\Delta\sigma(0)} = \frac{\Delta n(t) + n_{\text{hot}}(t)}{G\tau_{\text{th}} + G\left(\tau_r - \tau_{\text{th}}\tau_{\text{dtrp}} / \tau_{\text{trp}}\right)} \tag{14}$$

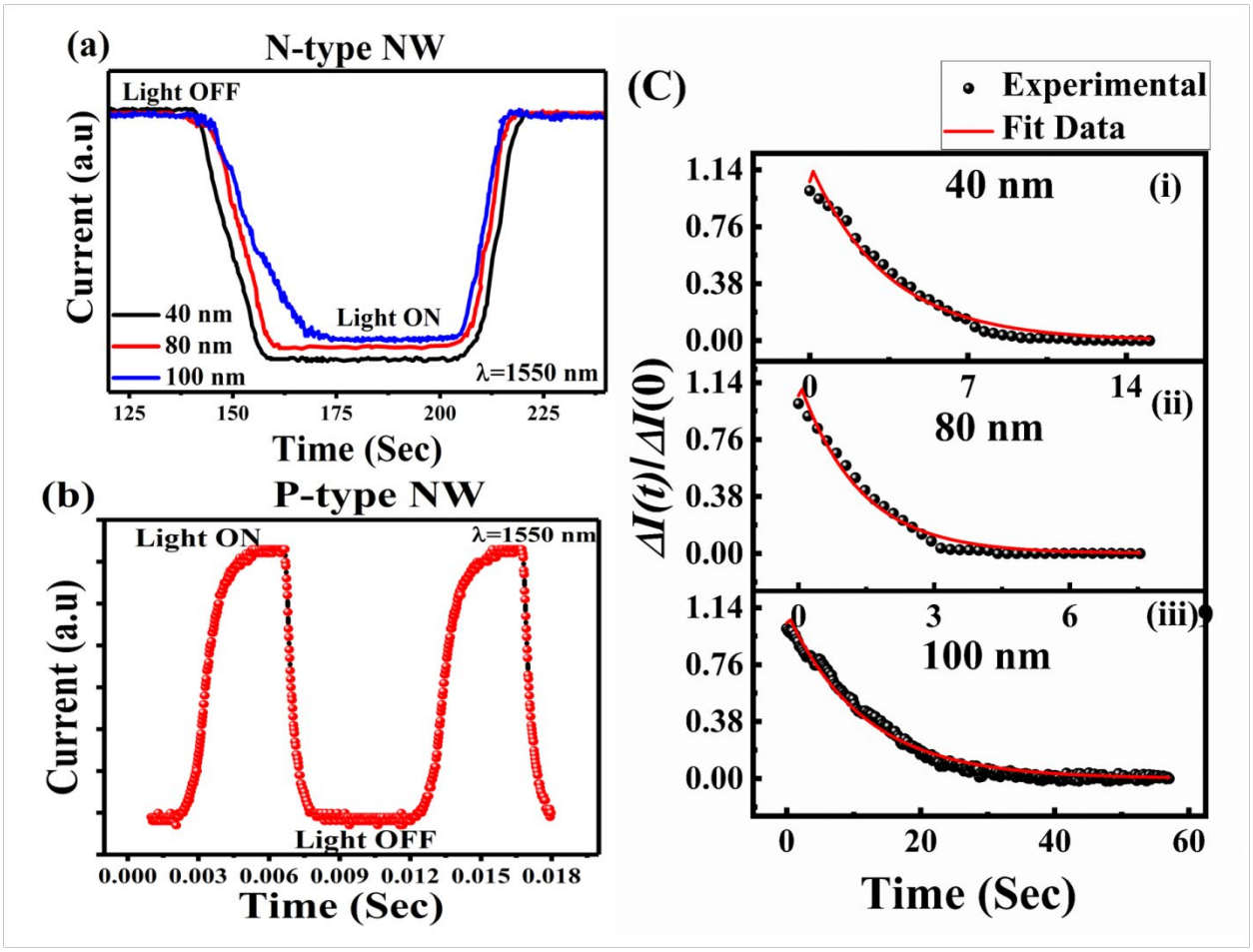

Fig. 6. Transient response. **a** n-type Ge NWs of different width, **b** p-type NW, and **c** Fitted curve of fall time with the experimental data for n-type NWs where the dotted line shows the experimental results and the solid line shows the fitted curve.

where $\Delta I(0)$ is the photocurrent at the moment of turning off the illumination. The above equations can be used to fit the photocurrent recovery following turning off the illumination. For the purpose of fitting the experimental data, we have assumed τ_{th} = 1 ps and τ_r = 10 ns[30]. The results of the fitting for n-type Ge NWs are shown in Fig. 6 (c) along with the transient response of Ge NWs in Fig. 6 (a) and (b). The values of the fitting parameters τ_{trp} and τ_{dtrp}, which are listed in Table 1, clearly shows that $\tau_{trp} < \tau_{dtrp}$ indicates that the free electrons generated as a result of illumination is being held by the trap states for more time, which is responsible for the NPC in n-type Ge NWs. As long as $\tau_{trp} < \tau_{dtrp}$, NPC will occur[13, 14]. Due to higher trapping and detrapping time as seen in Table 1, the n-type NWs show very slow photoresponse. In p-type NWs, switching speed depends upon the mobility of semiconductor and transit length which results in a fast response time.

Photodetector gain calculations. The internal gain of the n-type and p-type nanowires was calculated using following relation:[17, 32]

$$G_{ph} = \frac{N_{carrier}}{N_{photon}} = \frac{\frac{I_{ph}}{e}}{\frac{P_{absorb}}{h\omega}} \quad (15)$$

Here, $N_{carrier}$ is the number of carriers generated in the NW, N_{photon} is the number of photons absorbed by the NW, I_{ph} is the photocurrent ($I_{dark} - I_{light}$), e is the charge of the electron, h is the Planck's constant, ω is the frequency of the incident light and P_{absorb} is the power absorbed by the NW. Gain of both n-type and p-type nanowires as function of wavelength of incident light is shown in Fig. 7 (a) and (b). As incident photon energy is increased, the gain gradually increases and shows a peak at 1200 nm and then decreases. For lower wavelength (400-1200 nm) the absorption is high in Ge but at the same time the reflection losses are also high on reducing the incident light wavelengths and thus on increasing the wavelength from 400-1200 nm, the gain is increasing with reduced reflection losses. For the higher wavelength the absorption of Ge is less compared to smaller wavelength (~1200 nm) and thus the gain in low for larger wavelengths (1200 nm -1500 nm)[33, 34]. The factors except I_{ph} are not varying and therefore the trend is similar in n-type and p-type Ge NW despite their difference in photoconductive mechanism.

Table 1. Fitting parameters of n-type Ge NWs for different width.

Nanowire diameter (nm)	**τ_{trp} (Sec)**	**τ_{dtrp} (Sec)**
100	$(7.7 \pm 0.5)\times10^{-5}$	11.5 ± 0.1
80	$(1.2 \pm 0.2)\times10^{-5}$	1.34 ± 0.05
40	$(3.5 \pm 0.4)\times10^{-5}$	3.4 ± 0.1

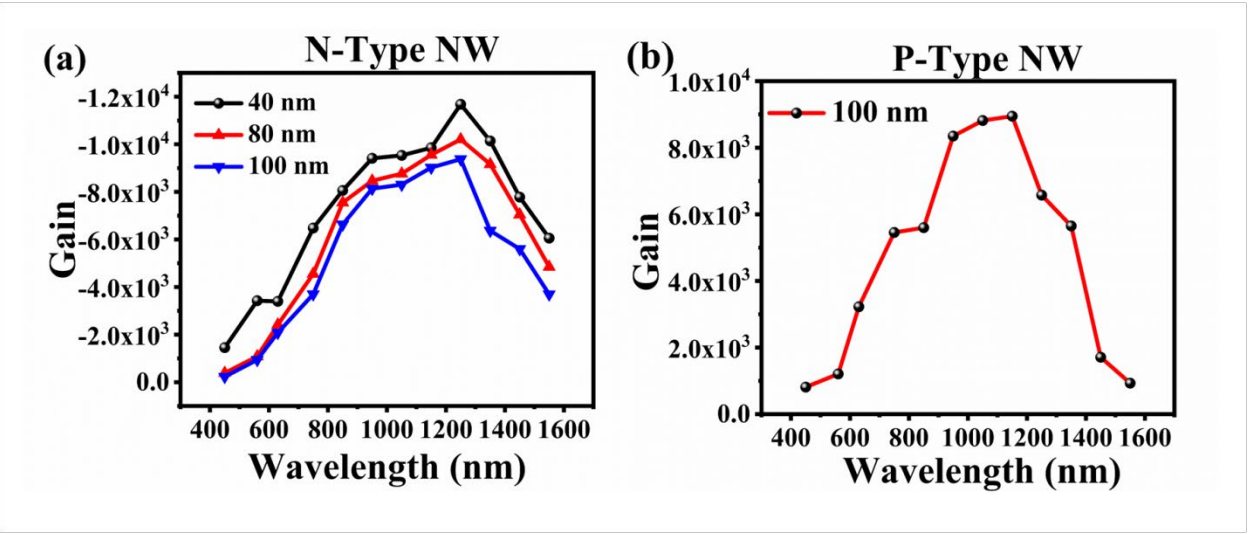

Fig. 7. Wavelength dependent gain of **a** n-type Ge NWs of different widths **b** p-type NWs. Very high gain of 10^4 order was observed for n-type and 9 x 10^3 for p-type Ge NWs.

Gain of both n-type and p-type nanowires as function of wavelength of incident light is shown in Fig. 7 (a) and (b). The maximum gain for both n and p-type devices was observed for 1250 nm of light. The gain also changes with NW diameter. Effective optical confinement in the thinner NWs results them in having higher optical absorption compared to that of thicker wires. The carrier dynamics in smaller wire is also affected by surface states and optical energy absorption per unit area of the device. The carrier recombination probability under optical illumination is reduced in NWs due to the trapping of carriers at surfaces states[20, 32]. The density of accumulated charge carriers Δn_{acc} at the surface of NWs increases the number of effective density (Δn_{eff}) of photogenerated carriers by the relation $\Delta n_{eff} = \Delta n + \Delta n_{acc}$. The total

density of surface accumulated carriers is related to nanowire diameter (surface to volume ratio) the relation:

$$\Delta n_{acc} \; \alpha \; \frac{2\pi(d/2)}{\pi(d/2)^2} \propto \frac{1}{d} \tag{16}$$

As the gain of the photodetector depends on the surface accumulated carrier density, diameter dependent gain is observed. The smallest diameter NW (40 nm) exhibits the highest photoconductive gain of 11,600 as shown in Fig. 7.

CONCLUSION

To summarize, we have reported diameter dependent negative photoconductive phenomenon in n-type Ge NWs and positive photoconductivity in p-type Ge NW for infrared light. This phenomenon was confirmed by measuring the contact potential from KPFM analysis where the CPD level decreases on account of incident light. The trapping and detrapping time calculated from the carrier trapping model suggest the same. NW MSM detector response to different wavelengths and intensity of light was investigated. The NW's were able to detect a wide wavelength range of incident light with maximum gain in ~ 10^4 order. The reported work can be made use in optoelectronic devices, specifically among multifunctional memory systems and low power communication applications.

AUTHOR INFORMATION

Corresponding Author

*E-mail: samaresh.das@care.iitd.ac.in

ORCID

*Samaresh Das: 0000-0003-4159-1962

Notes

The authors declare no competing financial interest.

ACKNOWLEDGEMENTS

The authors would like to thank Science and Engineering Research Board-Department of Science and Technology (SERB-DST), IMPacting Research Innovation and Technology (IMPRINT) and Science Foundation Ireland (Grant: 14/IA/2513) for financial support. Authors are very grateful to the Nanoscale Research Facility (NRF), IIT Delhi for providing assistance in the fabrication and characterization facilities.

REFERENCES

1. Hartmann, J. M.; Abbadie, A.; Papon, A. M.; Holliger, P.; Rolland, G.; Billon, T.; Fédéli, J. M.; Rouvière, M.; Vivien, L.; Laval, S. Reduced Pressure–Chemical Vapor Deposition of Ge Thick Layers on Si(001) for 1.3–1.55-Mm Photodetection. *Journal of Applied Physics* **2004**, *95* (10), 5905–5913.

2. Vivien, L.; Rouvière, M.; Fédéli, J.-M.; Marris-Morini, D.; Damlencourt, J. F.; Mangeney, J.; Crozat, P.; El Melhaoui, L.; Cassan, E.; Le Roux, X.; Pascal, D.; Laval, S. High Speed and High Responsivity Germanium Photodetector Integrated in a Silicon-On-Insulator Microwaveguide. *Opt. Express* **2007**, *15* (15), 9843.

3. Nam, D.; Sukhdeo, D.; Roy, A.; Balram, K.; Cheng, S.-L.; Huang, K. C.-Y.; Yuan, Z.; Brongersma, M.; Nishi, Y.; Miller, D.; Saraswat, K. Strained Germanium Thin Film Membrane on Silicon Substrate for Optoelectronics. *Opt. Express* **2011**, *19* (27), 25866.

4. Colace, L.; Masini, G.; Assanto, G. Ge-on-Si Approaches to the Detection of near-Infrared Light. *IEEE J. Quantum Electron.* **1999**, *35* (12), 1843–1852.

5. Jiang, X.; Li, S. S.; Tidrow, M. Z. Study of intersubband transition in quantum dots and quantum dot infrared photodetectors *Physica E: Low-dimensional Systems and Nanostructures*, **1999** *5*(1-2), 27-35.

6. Hsu, B.-C.; Chang, S. T.; Chen, T.-C.; Kuo, P.-S.; Chen, P. S.; Pei, Z.; Liu, C. W. A High Efficient 820 Nm MOS Ge Quantum Dot Photodetector. *IEEE Electron Device Lett.* **2003**, *24* (5), 318–320.

7. Ahn, Y. H.; Park, J. Efficient Visible Light Detection Using Individual Germanium Nanowire Field Effect Transistors. *Appl. Phys. Lett.* **2007**, *91* (16), 162102.

8. Soci, C.; Zhang, A.; Bao, X. Y.; Kim, H.; Lo, Y.; Wang, D. Nanowire Photodetectors. *Journal of nanoscience and nanotechnology,* **2010**, *10*(3), 1430-1449.

9. Huang, H. M.; Chen, R. S.; Chen, H. Y.; Liu, T. W.; Kuo, C. C.; Chen, C. P.; Hsu, H. C.; Chen, L. C.; Chen, K. H.; Yang, Y. J. Photoconductivity in Single AlN Nanowires by Subband Gap Excitation. *Appl. Phys. Lett.* **2010**, *96* (6), 062104.

10. Zhang, X.; Jie, J.; Wang, Z.; Wu, C.; Wang, L.; Peng, Q.; Yu, Y.; Jiang, P.; Xie, C. J. Surface induced negative photoconductivity in p-type ZnSe:Bi nanowires and their nano-optoelectronic applications. *Mater. Chem*. **2011**, 21 (18), 6736.

11. Li, L.; Auer, E.; Liao, M.; Fang, X.; Zhai, T.; Gautam, U. K.; Lugstein, A.; Koide, Y.; Bando, Y.; Golberg, D. Deep-ultraviolet solar-blind photoconductivity of individual gallium oxide nanobelts. *Nanoscale* **2011**, 3 (3), 1120.

12. Nakanishi, H.; Bishop, K. J. M.; Kowalczyk, B.; Nitzan, A.; Weiss, E. A.; Tretiakov, K. V.; Apodaca, M. M.; Klajn, R.; Stoddart, J. F.; Grzybowski, B. A. Photoconductance and Inverse Photoconductance in Films of Functionalized Metal Nanoparticles. *Nature* **2009**, 460 (7253), 371−375.

13. Yang, Y.; Peng, X.; Kim, H.-S.; Kim, T.; Jeon, S.; Kang, H. K.; Choi, W.; Song, J.; Doh, Y.-J.; Yu, D. Hot Carrier Trapping Induced Negative Photoconductance in InAs Nanowires toward Novel Nonvolatile Memory. *Nano Lett.* **2015**, *15* (9), 5875–5882.

14. Baek, E.; Rim, T.; Schütt, J.; Baek, C.; Kim, K.; Baraban, L.; Cuniberti, G. Negative Photoconductance in Heavily Doped Si Nanowire Field-Effect Transistors. *Nano Lett.* **2017**, *17* (11), 6727–6734.

15. Sze, S. M.; Ng. K. K. Physics of semiconductor devices, 3rd edition. *Wiley: Hoboken*, **2007.**

16. Ahn, Y.; Dunning, J.; Park, J. Scanning Photocurrent Imaging and Electronic Band Studies in Silicon Nanowire Field Effect Transistors. *Nano Lett.* **2005**, *5* (7), 1367–1370.

17. Nam, J. H.; Afshinmanesh, F.; Nam, D.; Jung, W. S.; Kamins, T. I.; Brongersma, M. L.; Saraswat, K. C. "Monolithic integration of germanium-on-insulator p-i-n photodetector on silicon," *Opt. Express,* **2015**, 23(12), 15816–15823.

18. Otuonye, U.; Kim, H. W.; Lu, W. D. Ge nanowire photodetector with high photoconductive gain epitaxially integrated on Si substrate *Appl. Phys. Lett.* **2017**, 110, 173104.

19. Sett, S.; Ghatak, A.; Sharma, D. K.; Kumar, G. V. P.; Raychaudhuri, A. K. Broad Band Single Germanium Nanowire Photodetectors with Surface Oxide-Controlled High Optical Gain *J. Phys. Chem. C* **2018**, 122, 8564.

20. Kim, C.-J.; Lee, H.-S.; Cho, Y.-J.; Kang, K.; Jo, M.-H. Diameter-Dependent Internal Gain in Ohmic Ge Nanowire Photodetectors. *Nano Lett.* **2010**, *10* (6), 2043–2048.

21. Gu, Y.; Kwak, E.-S.; Lensch, J. L.; Allen, J. E.; Odom, T. W.; Lauhon, L. J. Near-Field Scanning Photocurrent Microscopy of a Nanowire Photodetector. *Appl. Phys. Lett.* **2005**, *87* (4), 043111.

22. Gu, Y.; Romankiewicz, J. P.; David, J. K.; Lensch, J. L.; Lauhon, L. J. Quantitative Measurement of the Electron and Hole Mobility−Lifetime Products in Semiconductor Nanowires. *Nano Lett.* **2006**, *6* (5), 948–952.

23. Darken, L. S.; Hyder, S. A. Photoconductive Response of Compensating Impurities in Photothermal Ionization Spectroscopy of High-purity Silicon and Germanium. *Appl. Phys. Lett.* **1983**, *42* (8), 731–733.

24. Dhyani, V.; Das, S. High Speed MSM Photodetector Based on Ge Nanowires Network. *Semicond. Sci. Technol.* **2017**, *32* (5), 055008.

25. Wang, Y.; Liu, E.; Gao, A.; Cao, T.; Long, M.; Pan, C.; Zhang, L.; Zeng, J.; Wang, C.; Hu, W.; Liang, S.-J.; Miao, F. Negative Photoconductance in van der Waals Heterostructure-Based Floating gate Phototransistor. *ACS Nano*, **2018**, *12* (9), 9513-9520.

26. Sun, X.; Wang, X.; Wang, P.; Sheng, B.; Li, M.; Su, J.; Zhang, J.; Xu, F.; Yang, X.; Qin, Z.; Ge, W.; Shen, B. Identifying a doping type of semiconductor nanowires by photoassisted kelvin probe force microscopy as exemplified for GaN nanowires *Opt. Mater. Express* 7, **2017**, 904–912.

27. Glatzel, T.; Sadewasser, S.; Shikler, R.; Rosenwaks, Y.; Lux-Steiner, M. C. Kelvin probe force microscopy on III/V semiconductors: the effect ofsurface defects on the local work function*Mat. Sci. Eng. B*, **2003**, 102, P.138.

28. Greytak, A. B.; Lauhon, l. J.; Gudiksen, M. S.; Lieber, C. M Growth and transport properties of complementary germanium nanowire field effect transistors *Appl. Phys. Lett*. **2004** 84, 4176.

29. Piro, M.-C.; Broniatowski, A.; Marnieros, S.; Dumoulin, L.; Olivieri, E. Hot Carrier Trapping in High-Purity and Doped Germanium Crystals at Millikelvin Temperatures. *J Low Temp Phys* **2014**, *176* (5–6), 796–801.

31. Costato, M.; Fontanesi, S.; Reggiani, L. Electron energy relaxation time in Si and Ge *J. Phys. Chem. Solids* **1973**, 34 (3), 547−564.

32. Dhyani, V.; Jakhar, A.; Wellington J, J.; Das, S. Diameter-Dependent Photoresponse with High Internal Gain in a Back Gated Single Si Nanowire Phototransistor. *J. Phys. D: Appl. Phys.* **2019**, *52*.

33. Colace, L.; Assanto, G. Germanium on Silicon for Near-Infrared Light Sensing *IEEE photonics Journal,* **2009**, 1 (2), 69 – 79.

34. Wang, K. L.; Cha, D.; Liu, J.; Chen, C. Ge/Si Self-Assembled Quantum Dots and Their Optoelectronic Device Applications, *Proceedings of the IEEE*, **2007**, 95 (9), 1866 – 1883.

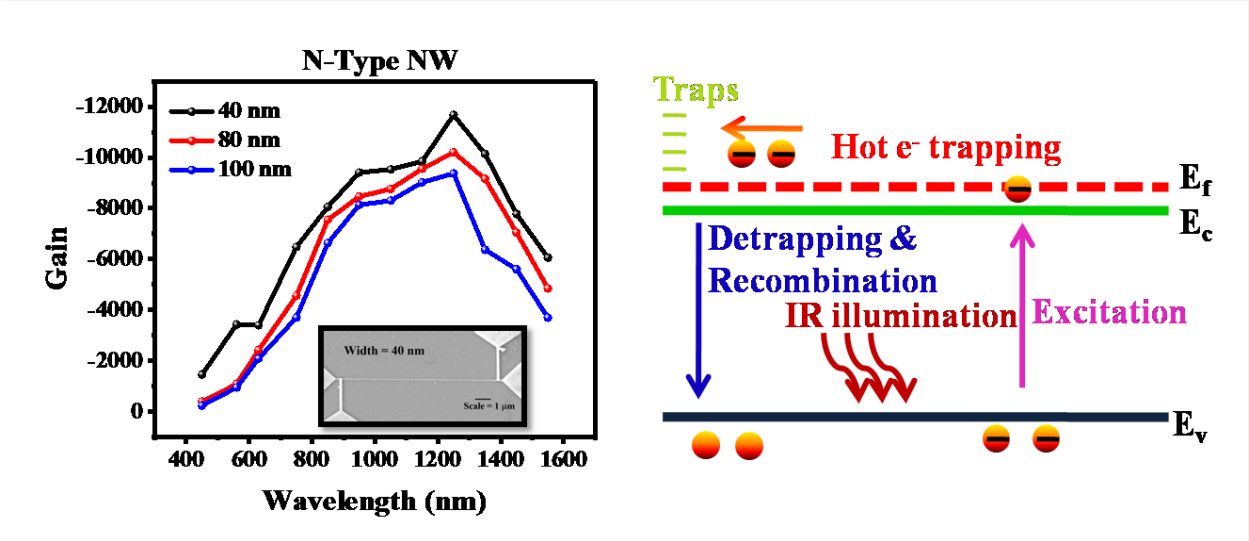

Fig: Table of Contents Graphic